Available online at www.sciencedirect.com
ScienceDirect
Journal of Sound and Vibration 322 (2009) 808–828
JOURNAL OF SOUND AND VIBRATION
www.elsevier.com/locate/jsvi

Laminar boundary layer instability noise produced by an aerofoil

Michael J. Kingan*, John R. Pearse

Department of Mechanical Engineering, University of Canterbury, Christchurch, New Zealand

Received 2 May 2007; received in revised form 6 March 2008; accepted 23 November 2008
Handling Editor: L.G. Tham

Abstract

When a laminar boundary layer exists on the surface of an aerofoil up to the trailing edge, a tone or a number of tones are sometimes produced. These tones have been the subject of a number of investigations which have proposed a variety of different mechanisms regarding their production. This paper gives a brief overview of the previously proposed mechanisms and then describes the development of a theoretical model to estimate the tone frequencies. The model is validated against a number of well-known published experiments and also against the results of an experimental investigation undertaken by the authors. The model is compared with other models available for predicting laminar boundary layer instability noise and is shown to be accurate and robust. Unlike previous models, which are empirical, the model presented in this paper is purely theoretical and could be used to predict the frequency of laminar boundary layer instability noise produced by an arbitrary aerofoil.

1. Introduction

When a laminar boundary layer exists on one surface (usually the pressure surface) of an aerofoil up to the trailing edge, in certain instances a tone or a number of high amplitude tones are produced. The first comprehensive study on noise generated in this way was done by Paterson et al. [1] who attributed the tonal noise produced by the aerofoils to vortex shedding from the trailing edge. Paterson et al. [1] observed that the 'peak frequency', f_s, of the noise produced by the interaction of airflow with the aerofoil scaled approximately according to the following relationship:

$$f_s = 0.011 U_\infty^{1.5} (Cv)^{-0.5} \tag{1}$$

where U_∞ is the free-stream airflow speed, C is the aerofoil chord and v is the kinematic viscosity of air. Paterson et al. [1] observed that the presence of the tone was associated with a laminar boundary layer existing up to the trailing edge of the aerofoil. Also, they found that the sound radiated from the trailing edge exhibited a ladder type variation for small variations in the free stream velocity U_∞ and that the frequency of the tones

*Corresponding author.
E-mail address: mk@isvr.soton.ac.uk (M.J. Kingan).

0022-460X/$ - see front matter © 2008 Elsevier Ltd. All rights reserved.
doi:10.1016/j.jsv.2008.11.043

on each rung of the ladder was approximately proportional to $U_\infty^{0.8}$. It was also observed that a number of tones at different frequencies could exist at one flow velocity, see Fig. 1.

Tam [2] proposed that the source of the tonal noise was a self-excited feedback loop between the point of first instability (the point at which the boundary layer first becomes unstable) on the surface of the aerofoil and a point downstream in the wake. Tam's model is outlined below.

Laminar boundary layer instabilities, known as Tollmien–Schlichting waves (T–S waves, see Ref. [3]), become amplified as they move over the aerofoil surface. Upon reaching the trailing edge these instabilities propagate into the wake where they cause the wake to vibrate laterally. These wake vibrations emit an acoustic wave which propagates upstream and reinforces the original disturbance completing the feedback loop. The loop is maintained if the sound has appropriate phase and magnitude to couple with the boundary layer instability waves at the source (the point of first instability). Tam's [2] proposed feedback mechanism was modified by a number of other investigators including Wright [4], Longhouse [5], Fink [6] and Arbey and Bataille [7].

As Tam [2] and most subsequent investigators assume that the tones are in some way produced by laminar boundary layer instabilities, the tonal noise generation mechanism will be referred to as 'laminar boundary layer instability noise' (as per Refs. [8,9]). Although other investigators refer to the same phenomenon as laminar boundary layer vortex shedding noise (e.g., [10]).

Arbey and Bataille [7] conducted a comprehensive experimental and theoretical investigation on the noise generated by an aerofoil immersed in a laminar flow and found that the spectrum consisted of a broadband contribution which peaked at f_s and a discrete contribution at equidistant frequencies f_n. They concluded that the broadband contribution could be attributed to the diffraction of hydrodynamic instabilities (T–S waves) in the developing boundary layer by the trailing edge, whereas the equi-spaced discrete frequencies were due to an aeroacoustic feedback loop, between the aerofoil trailing edge and the point of first instability. Arbey and Bataille's proposed feedback loop is summarized in Fig. 2.

As the frequency of the boundary layer instabilities scale with the boundary layer thickness, Arbey and Bataille [7] proposed that the frequency of the broadband noise scaled with $U_\infty^{1.5}$ consistent with the

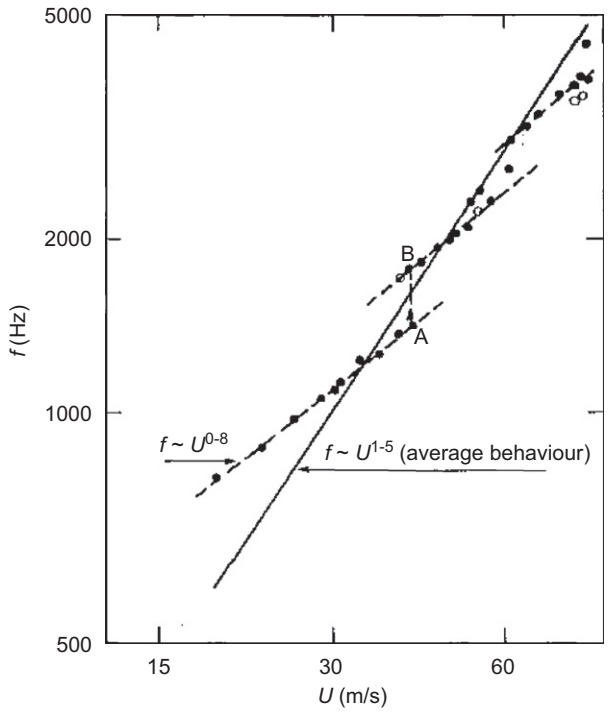

Fig. 1. Ladder-type frequency relationship observed by Paterson et al. [1] (from Ref. [7]).

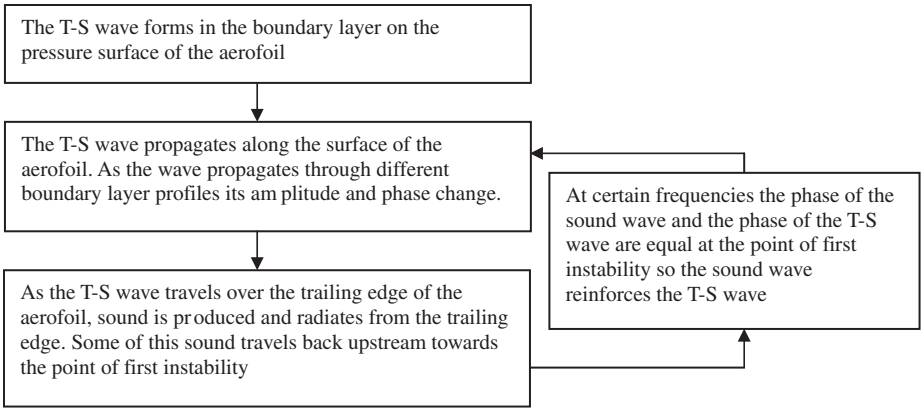

Fig. 2. Flow diagram of the feedback loop proposed by Arbey and Bataille [7].

observations and analysis of Paterson et al. [1]. They formulated an empirical relationship for f_s based on the analysis of experimental data from tests on a number of different aerofoils.

$$f_s = \frac{St_s U_\infty}{\delta^*_{\mathrm{TE}}} \tag{2}$$

In Eq. (2) St_s was determined to be 0.048 ± 0.003 and δ^*_{TE} is the displacement thickness at the trailing edge of the aerofoil (which was calculated using the method of Mari et al. [11]). Arbey and Bataille [7] also found Eq. (2) to be in reasonable agreement with Eq. (1).

Arbey and Bataille [7] proposed f_n could be determined from the following relationship:

$$\frac{f_n L_A}{c_r}\left(1 + \frac{c_r}{c_0 - U_\infty}\right) = n + \frac{1}{2}, \quad n = 1, 2, 3, \ldots \tag{3}$$

where L_A is defined as the distance between the point of maximum velocity over the aerofoil surface and the trailing edge (which was calculated using the method of Henry [12]), c_r is the propagation speed of the T–S wave, c_0 is the speed of sound and U_∞ is the free-stream airflow speed. They also give an empirical formula for calculating the frequency spacing between the tones Δf

$$\Delta f = \frac{K U^m}{L_A} \tag{4}$$

In Eq. (4) $K = 0.89 \pm 0.05$ and $m = 0.85 \pm 0.01$. For laminar boundary layer instability noise Arbey [13] confirmed the source of the sound was close to the trailing edge using an acoustic imaging technique. This source of sound was proposed by Arbey and Bataille [7] to be caused by the diffraction of T–S waves around the sharp trailing edge of the aerofoil.

The sound produced by instability waves has been studied by Dolgova [14], Akylas and Toplosky [15], Laufer and Yen [16] and Crighton and Hueere [17]. Aizin [18] investigated the generation of sound by a T–S wave which convects over the trailing edge of a very thin flat plate. The analysis considered the diffraction of a T–S wave at the end of a flat plate in a uniform flow. Aizin derived an analytical expression for the acoustic radiation into the far field. The analysis showed that the sound field had the same frequency as the T–S wave in the boundary layer and was directly proportional to the pressure exerted by the T–S wave at the sharp edge.

Archibold [19] also investigated the development of T–S waves on the surface of an aerofoil spanning the working section of a low speed wind tunnel. It was found that the T–S waves were the source of excitation of standing waves within the tunnel. The acoustic waves excited the growth of T–S waves from the point of first instability on the aerofoil surface. The T–S waves then became amplified as they passed over the surface of the aerofoil and produced sound as they convected over the trailing edge. The feedback loop proposed by Archibald is quite similar to that proposed by Arbey and Bataille [7] (except that feedback is provided by acoustic standing waves in the tunnel rather than acoustic waves propagating upstream from the trailing edge).

Using linear stability analysis and experimental measurements of the boundary layer profiles over the pressure surface of an aerofoil, McAlpine et al. [8] and Nash et al. [9] were able to calculate the total amplification of T–S waves over the pressure surface of an aerofoil. They proposed that the frequency of the tonal noise was identical to the frequency of the T–S wave that underwent maximum amplification over the aerofoil surface and that the majority of amplification occurred across a small separation bubble close to the trailing edge which was present in the cases they were investigating. McAlpine et al. [8] proposed the following tone selection mechanism "the tones may simply be explained in terms of the amplification of boundary layer instabilities and we believe that a feedback mechanism is not a necessary condition for the generation of tonal noise … however, the coupling between the boundary layer instabilities and the wake instabilities together with an upstream feedback mechanism about the separation bubble provides a mechanism which results in the narrow band spectral characteristics of the acoustic tone."

Brooks et al. [10] give an expression for determining the peak frequency f_s produced by an aerofoil exhibiting laminar boundary layer instability noise. They provide an empirical model that can be used for predicting the peak frequency of the laminar boundary layer instability noise produced by an NACA0012 aerofoil. The model is only really applicable to cases where the NACA0012 aerofoil is used. However, their model is compared with the model presented here and with the experimental results of the other investigators. For completeness the model is given fully in Appendix A.

An experimental investigation undertaken by the authors indicated that a feedback mechanism similar to that proposed by Arbey and Bataille [7] was producing laminar boundary layer instability noise on aerofoils immersed in an airflow (the sound pressure spectrum produced by the aerofoils exhibited a broadband hump with a number of evenly spaced tones). The aerofoils being investigated were relatively thick (18–30 percent thickness to chord ratios) and as the model of Brooks et al. [10] was empirical and based only on tests using a NACA0012 aerofoil the applicability of their model for predicting the frequency of laminar boundary layer instability noise was questioned.

This paper describes an accurate and purely theoretical method of calculating the frequency of laminar boundary layer instability tones produced by an aerofoil according to Arbey and Batille's feedback loop. In Section 2 a method, based on that proposed by McAlpine et al. [8] and Nash et al. [9], to calculate the amplification of a T–S wave over the surface of an aerofoil using an easily automated method of solving the Orr–Sommerfeld equation is described. A model based on the feedback mechanism proposed by Arbey and Bataille [7] is then developed. While in Section 3 the model is validated against a number of published experiments and also against the results of an experimental investigation undertaken by the authors. A number of recommendations are made in Section 4.

The motivation for this work came from a desire to predict the presence of tones produced by an automobile 'roof rack' cross-bar, which resembled a thick aerofoil. The final method can be used to predict the frequency of laminar boundary layer instability tones and could possibly be incorporated into a general method for the prediction of aerofoil tone noise, such as Ref. [10]. Possible applications occur when the noise produced by an aerofoil in a low-Reynolds number flow are of concern e.g. automobile roof racks and micro wind-turbines.

2. Modelling T–S wave propagation

2.1. Mean flow calculation

The growth of the boundary layer over the surface of the aerofoil was modelled using the XFOIL software package. XFOIL is a coupled potential flow solver and boundary layer integral method. The general XFOIL methodology is described in Ref. [20], while the boundary layer formulation is described in Ref. [21]. XFOIL was selected because of its ability to very quickly and accurately determine boundary layer profiles on an aerofoil surface even for mildly separated flows.

The boundary layer displacement thickness δ^* and shape factor H were calculated at stations located at 2 percent chord intervals from the leading edge to the trailing edge of the aerofoil. The boundary layer velocity profile at each station was defined as the Falkner–Skan velocity profile with an identical shape factor to that calculated using XFOIL (the XFOIL laminar boundary layer formulation assumes a Falkner–Skan boundary

layer profile). The Falkner–Skan boundary layer is described by the following equations:

$$f''' + ff'' + \beta(1 - f'^2) = 0 \tag{5}$$

$$f(0) = f'(0) = 0, \quad \lim_{\eta\to\infty} f'(\eta) \to 1 \tag{6}$$

In Eqs. (5) and (6) f' is the dimensionless velocity profile (non-dimensionalized by the local free stream velocity) and the prime denotes differentiation with respect to the dimensionless coordinate η which is defined $\eta = \hat{\eta}/L$ where L is a length scale which is defined below:

$$L = \frac{\delta^*}{\gamma}, \quad \gamma = \int_0^\infty (1 - f')\,\mathrm{d}\eta \tag{7}$$

In Eq. (7) δ^* is the dimensional boundary layer displacement thickness and f' is the dimensionless Falkner–Skan velocity profile with the same shape factor H as the boundary layer under consideration ($H = \delta^*/\theta$, where θ is the boundary layer momentum thickness).

The Orr–Sommerfeld equation requires the boundary layer velocity profile to be determined accurately. For the cases presented in this paper the boundary layer profiles were determined by solving the Falkner–Skan equation using the parallel shooting technique described by Cebeci and Keller [22] employing a fourth order Runge–Kutta–Gill solver.

2.2. Stability analysis

Following the method described in Refs. [8,9] it is assumed that the two-dimensional T–S waves can be modeled by spatial modes of fixed frequency with slowly changing wavelengths. The stream function $\psi(\hat{\xi}, \hat{\eta}, t)$ of these T–S waves is described by the following expression:

$$\psi(\hat{\xi}, \hat{\eta}, t) = \phi(\hat{\eta})\, \mathrm{e}^{\mathrm{i}\left(\int \hat{\alpha}(\hat{\xi})\,\mathrm{d}\hat{\xi} - \hat{\omega}t\right)} \tag{8}$$

In Eq. (8) $\mathrm{i} \equiv \sqrt{-1}$, t is time, ϕ is the perturbation amplitude and $\hat{\eta}$ is the stream-normal coordinate. The complex wavenumber $\hat{\alpha}$ is assumed to vary slowly with the streamwise coordinate $\hat{\xi}$ and the wavenumber of the least stable mode at a point along the surface of the aerofoil is calculated for a given velocity profile U, Reynolds number R and frequency $\hat{\omega}$ by solving the Orr–Sommerfeld equation

$$(U\alpha - \omega)(\phi'' - \alpha^2\phi) - U''\alpha\phi + \frac{\mathrm{i}}{R}(\phi^{iv} - 2\alpha^2\phi'' + \alpha^4\phi) = 0 \tag{9}$$

The prime denotes differentiation with respect to the dimensionless coordinate $\eta = \hat{\eta}/L$, $R = U_\infty L/\nu$ is the Reynolds number, here U_∞ is the local free-stream velocity and the variables in the Orr–Sommerfeld equation are all non-dimensional i.e.,

$$\alpha = \hat{\alpha}L, \quad U = \hat{U}/U_\infty, \quad \omega = \hat{\omega}L/U_\infty, \quad c = \hat{c}/U_\infty \tag{10}$$

The hat indicates the dimensional variable. For boundary layer flow Eq. (9) is subject to the following boundary conditions:

$$\eta = 0, \quad \phi = 0, \quad \phi' = 0 \tag{11a}$$

$$\lim_{\eta\to\infty}, \quad \phi = 0, \quad \phi' = 0 \tag{11b}$$

The Orr–Sommerfeld problem defined by Eqs. (9), (11a) and (11b) describes the development of infinitesimal disturbances in a boundary-layer flow with velocity profile $U(\eta)$. The Orr–Sommerfeld equation may be solved for fixed (R,ω) to determine the wavenumber α of the least stable mode at any point in the (R,ω) plane. The Orr–Sommerfeld problem was solved using a Chebyshev matrix technique which is described below.

2.3. Numerical method

For the spatial stability case the eigenvalue appears to the fourth power in the Orr–Sommerfeld equation. To reduce the order of the eigenvalue problem from a fourth order problem to a second order problem a transformation is introduced (following Haj-Hariri [23])

$$\phi = \Phi \mathrm{e}^{-\alpha\eta} \tag{12}$$

The reduced Orr–Sommerfeld equation is thus

$$(\mathrm{i}\omega - \mathrm{i}\alpha U)(\Phi'' - 2\alpha\Phi') + \mathrm{i}U''\alpha\Phi + \frac{1}{R}(\Phi^{iv} - 4\alpha\Phi''' + 4\alpha^2\Phi'') = 0 \tag{13}$$

with the same boundary conditions as Eqs. (11a) and (11b) with ϕ replaced by Φ. The transformed perturbation amplitude $\Phi(\eta)$ was approximated by a series of Chebyshev polynomials $T_n(x)$:

$$\Phi(\eta) = \sum_{n=0}^{N} a_n T_n(x), \quad \text{where } T_n(x) = \cos(n\cos^{-1}(x)) \tag{14}$$

The Chebychev polynomials were defined on the interval $(-1 \leqslant x \leqslant 1)$ at the Gauss–Lobbotto collocation points x_i:

$$x_i = \cos\left(\frac{\pi i}{N}\right), \quad i = 0, \ldots, N \tag{15}$$

The derivatives of Φ were found by differentiating the coefficients a_n through the use of derivative operators $\hat{\mathbf{D}}$:

$$\Phi^k(\eta_i) = \sum_{j=0}^{N} \hat{\mathbf{D}}_{ij}^k a_j T_j(x_i) \tag{16}$$

The derivative operator $\mathbf{D}$ on the Chebyshev domain $(-1 \leqslant x \leqslant 1)$ and can be constructed in matrix form (see for example Ref. [24])

$$\mathbf{D}_{00}^1 = -\mathbf{D}_{NN}^1 = \frac{2N^2+1}{6}, \quad \mathbf{D}_{ii}^1 = -\frac{\eta_i}{2(1-\eta_i^2)} \tag{17}$$

$$\mathbf{D}_{ij}^1 = -\frac{c_j(-1)^{i+j}}{c_i(\eta_j - \eta_i)} \quad \text{if } i \neq j, \ c_0 = 2 \text{ and } c_i = 1 \tag{18}$$

Higher order derivative operators are defined

$$\mathbf{D}^k = (\mathbf{D}^1)^k \tag{19}$$

The derivative operators $\mathbf{D}^k$ are defined on the Chebyshev domain $(-1 \leqslant x \leqslant 1)$ and are required to be mapped onto the semi-infinite domain $(0 \leqslant \eta \leqslant \infty)$. This was done using an algebraic transformation (see for example Ref. [25]):

$$\eta_j = l\frac{1-x_j}{1+s+x_j} \tag{20}$$

where η_j is the jth Gauss–lobotto point x_j transformed to the semi-infinite domain. In this study it was found that $s = 2$ and $l = 50$ provided stable results. It should be noted that this transformation truncates the domain at $\eta = l$, and thus the boundary conditions described by Eq. (11b) are applied at $\eta = l$ rather than at infinity. The good agreement between results obtained using the current method and the results obtained using the method of Ng and Reid [26], who correctly apply the upper boundary condition, indicates that the truncation of the domain does not significantly affect the accuracy of the method. Applying the chain rule to the derivative matrices $\mathbf{D}^k$, the derivative matrices for the semi-infinite domain, $\hat{\mathbf{D}}^k$ are

$$\hat{\mathbf{D}}_{ij}^1 = \frac{\mathrm{d}x}{\mathrm{d}\eta}\mathbf{D}_{ij}^1, \quad \hat{\mathbf{D}}_{ij}^2 = \left(\frac{\mathrm{d}x}{\mathrm{d}\eta}\right)^2 \mathbf{D}_{ij}^2 + \frac{\mathrm{d}^2x}{\mathrm{d}\eta^2}\mathbf{D}_{ij}^1 \tag{21}$$

$$\hat{\mathbf{D}}_{ij}^3 = \left(\frac{\mathrm{d}x}{\mathrm{d}\eta}\right)^3 \mathbf{D}_{ij}^3 + 3\frac{\mathrm{d}^2x}{\mathrm{d}\eta^2}\frac{\mathrm{d}x}{\mathrm{d}\eta}\mathbf{D}_{ij}^2 + \frac{\mathrm{d}x^3}{\mathrm{d}\eta^3}\mathbf{D}_{ij}^1 \tag{22}$$

$$\hat{\mathbf{D}}_{ij}^4 = \left(\frac{\mathrm{d}x}{\mathrm{d}\eta}\right)^4 \mathbf{D}_{ij}^4 + 6\frac{\mathrm{d}^2x}{\mathrm{d}\eta^2}\left(\frac{\mathrm{d}x}{\mathrm{d}\eta}\right)^2 \mathbf{D}_{ij}^3 + \left(3\left(\frac{\mathrm{d}^2x}{\mathrm{d}\eta^2}\right)^2 + 4\frac{\mathrm{d}^3x}{\mathrm{d}\eta^3}\frac{\mathrm{d}x}{\mathrm{d}\eta}\right)\mathbf{D}_{ij}^2 + \frac{\mathrm{d}x^4}{\mathrm{d}\eta^4}\mathbf{D}_{ij}^1 \tag{23}$$

where the derivatives $\mathrm{d}x/\mathrm{d}\eta$, $\mathrm{d}^2x/\mathrm{d}\eta^2$, etc. are all evaluated at η_i. Substituting the series representation for Φ (Eq. (16)) into the reduced Orr–Sommerfeld eigenvalue problem (Eq. (13)) yields the following second order eigenvalue problem

$$(\mathbf{A}\alpha^2 + \mathbf{B}\alpha + \mathbf{C})\Phi = 0 \tag{24}$$

where

$$\mathbf{A} = 2\mathbf{U}\hat{\mathbf{D}} + 4\hat{\mathbf{D}}^2/R \tag{25}$$

$$\mathbf{B} = -2\mathrm{i}\omega\hat{\mathbf{D}} - \mathrm{i}\mathbf{U}\hat{\mathbf{D}}^2 + \mathrm{i}\mathbf{U}'' - 4\hat{\mathbf{D}}^3/R \tag{26}$$

$$\mathbf{C} = \mathrm{i}\omega\hat{\mathbf{D}}^2 + \hat{\mathbf{D}}^4/R \tag{27}$$

and where $\mathbf{U}$ and $\mathbf{U}''$ are diagonal matrices with $\mathbf{U}_{ii} = U(\eta_i)$ and $\mathbf{U}''_{ii} = U''(\eta_i)$ being, respectively, the velocity U and its second derivative U'' at the transformed Gauss–Lobotto points η_i.

Boundary conditions are applied to the first and last two rows of $\mathbf{A}$, $\mathbf{B}$ and $\mathbf{C}$. Following Bridges and Morris [27], the eigenvalues of the companion matrix are the roots of the corresponding polynomial equation, a companion matrix for Eq. (24) can be written as

$$\left\{\begin{bmatrix} -\mathbf{B} & -\mathbf{C} \\ \mathbf{I} & 0 \end{bmatrix} - \alpha\begin{bmatrix} \mathbf{A} & 0 \\ 0 & \mathbf{I} \end{bmatrix}\right\}\begin{bmatrix} \alpha\Phi \\ \Phi \end{bmatrix} = 0 \tag{28}$$

This equation represents a complex generalized eigenvalue problem and can be solved by the QZ algorithm. The advantage of the method is it is quick, accurate and identifies a number of T–S modes from which the least stable can be identified. Unlike local solvers the method requires no initial guess of the value of the least stable mode and is thus well suited to automation.

The method returns a spectrum of eigenvalues which contains (1) eigenvalues corresponding to T–S modes, (2) pseudo-eigenvalues and (3) finite approximations to the continuous spectrum in the complex α-plane (see for example Ref. [28]). As only eigenvalues which correspond to growing T–S waves are desired, the eigenvalues which do not correspond to T–S waves are removed by searching only for the least stable eigenvalue (minimum α_i) between $0.2 < \alpha_i < 0$ and $0 < \alpha_r < 30$. The method appears to be robust and accurate and was used to plot curves of constant spatial amplification for the Blasius boundary layer (Fig. 3).

Note that the Blasius boundary layer velocity profile is given by setting $\beta = 0$ in Eq. (5) and dividing the non-dimensional stream-normal coordinate η by two. Also, all lengths are non-dimensionalized by δ^*, rather than L, i.e., $R_{\delta^*} = U_\infty\delta^*/\nu$ and $\omega_{\delta^*} = \hat{\omega}\delta^*/U_\infty$.

The least stable T–S mode calculated using the method described here is compared with the calculation of Jordinson [29] in Table 1.

2.4. Wind tunnel corrections

For tests conducted on an aerofoil immersed in a free-jet, because of the finite size of the free-jet, the pressure distribution over the aerofoil is slightly different to that of an aerofoil in free space. Therefore a 'free equivalent aerofoil', which had the same surface pressure distribution as the aerofoil in the wind tunnel, was calculated using the method of Brooks and Marcolini [30]. For tests conducted in a closed wind tunnel, a solid blockage correction was applied to the measured wind tunnel velocity, and an equivalent free aerofoil was calculated using the method of Allen and Vincenti [31]. Both methods described in Refs. [30,31] apply a correction to the camber-line of the aerofoil, which converts the aerofoil to the 'free equivalent aerofoil'. The

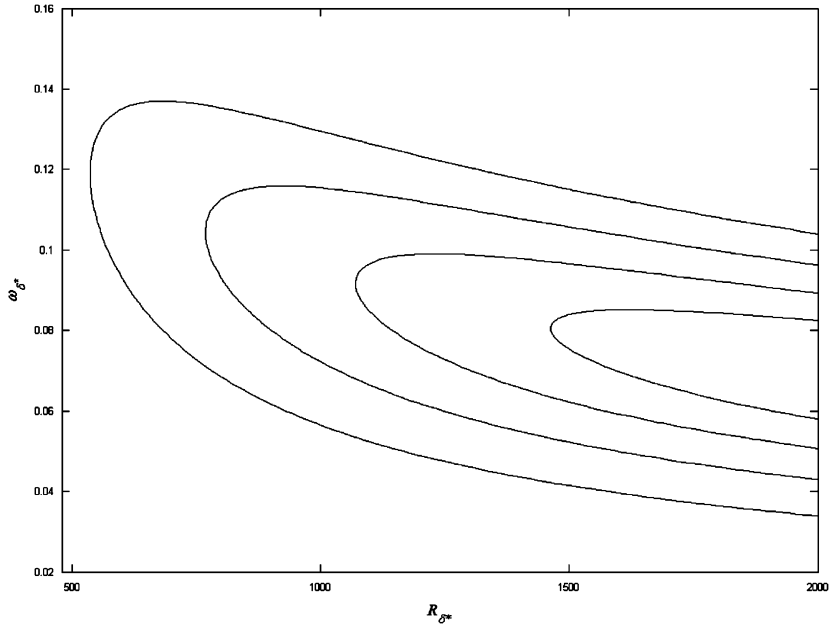

Fig. 3. Contours of constant spatial amplification for Blasius boundary layer flow determined using the method described here (the outer curve corresponds to the $\alpha_i = -5 \times 10^{-4}$).

Table 1
Validation of the method for predicting least stable T–S mode.

R_{δ^*}	ω_{δ^*}	Jordinson	Method presented in this paper
598	0.1297	0.3079–0.0019i	0.30784–0.00190i
998	0.1122	0.3086–0.0057i	0.30859–0.00571i

thickness distribution is assumed to remain the same. Details of the wind tunnel corrections can be found in the references given above.

2.5. T–S wave amplification

The total amplification A of a T–S wave with slowly varying complex wavenumber between $\hat{\xi} = a$ and $\hat{\xi} = b$ (where b is downstream of a) over the aerofoil surface S is

$$A = \exp\left(- \int_a^b \hat{\alpha}_i(\hat{\xi}) \, \mathrm{d}S(\hat{\xi}) \right) \tag{29}$$

The integral in Eq. (29) was evaluated using the rectangle rule. The T–S wavenumber $\hat{\alpha}$ was evaluated at 2 percent chord intervals from the leading edge to the trailing edge.

McAlpine et al. [8] noted that the general method makes several assumptions which may compromise the accuracy of the calculations in certain circumstances. In the Orr–Sommerfeld problem it is assumed that the flow is parallel, which is a reasonable assumption when the boundary layer growth is relatively small. However, in regions where the boundary layer thickness increases rapidly the calculations will become inaccurate. Also, for flows where the separation becomes very large, the boundary layer equations may become invalid. The model therefore is only applicable when separation is located close to the trailing edge of the aerofoil, and the height of the region of reversed flow remains relatively small.

2.6. Extension of the model to include a tone selection mechanism

By solving the Orr–Sommerfeld equation at a number of stations over the aerofoil surface, the phase change between the point of first instability and the trailing edge can be calculated at a particular frequency. The model is based on the feedback loop proposed by Arbey and Bataille [7] and is used to evaluate their proposed feedback mechanism against published experimental results in Section 3. It should be noted that Arbey and Bataille [7] include a similar feedback model in their work, however the exact details of the calculation of the variation of the T–S wave phase over the surface of the aerofoil was not clear.

Assuming that sound is produced at the trailing edge and propagates upstream outside the boundary layer to the point of first instability, by calculating the phase change of both the sound and the T–S wave around the feedback loop, the frequency at which T–S waves will become reinforced and produce tonal noise may be calculated. The total phase change around the feedback loop may be deduced by considering each component of the loop separately.

Considering first the phase change of the T–S wave as it propagates downstream along the aerofoil surface. The phase change between each station can be calculated by solving the Orr–Sommerfeld equation at each station. From this the total phase change between the point of first instability and the trailing edge can be calculated at a particular frequency. From inspection of the stream function of the T–S wave (Eq. (8)) the phase change over the aerofoil surface S between the point of first instability (at $\hat{\xi} = a$) and the trailing edge (at $\hat{\xi} = b$) is

$$\int_a^b \hat{\alpha}_r(\hat{\xi})\,\mathrm{d}S(\hat{\xi}) \tag{30}$$

The integral in Eq. (30) is a function of frequency and was evaluated using the rectangle rule at a number of discrete frequencies.

According to Arbey and Bataille [7], diffraction of the T–S wave around the trailing edge results in a 180° (π radians) phase shift which must be added to the total phase change around the feedback loop (this was observed in the experiments of Yu and Tam [32]). The sound wave generated at the trailing edge then propagates back upstream at a speed of approximately $c_0 - U_{\infty,L}$, where c_0 is the speed of sound relative to the fluid and $U_{\infty,L}$ is the average free-stream airflow speed over the surface of the aerofoil between the trailing edge ($x_1 = b$) and the point of first instability ($x_1 = a$). The phase change of the sound wave is thus

$$\frac{2\pi f L}{c_0 - U_{\infty,L}} \tag{31}$$

In Eq. (31) L is the distance along the aerofoil surface between points a and b. At each frequency the point of first instability, a, was taken to be the first station where α_i became negative. The total phase change around the feedback loop is thus

$$\int_a^b \hat{\alpha}_r(\hat{\xi})\,\mathrm{d}S(\hat{\xi}) + \pi + \frac{2\pi f L}{c_0 - U_{\infty,L}} \tag{32}$$

When this expression is equal to a multiple of 2π the acoustic wave will reinforce the T–S wave at the point of first instability and will result in a tone being produced, i.e., tones will occur at frequencies at which the following relationship is satisfied:

$$\frac{1}{2\pi}\int_a^b \hat{\alpha}_r(x_1)\,\mathrm{d}x_1 + \frac{1}{2} + \frac{fL}{c_0 - U_{\infty,L}} \equiv F(f) = n, \quad n = 1, 2, 3\ldots \tag{33}$$

In the current method the phase function $F(f)$ was calculated over the range of frequencies for which T–S wave amplification occurs. A least squares parabola was fitted to $F(f)$ and frequencies which satisfied $F(f) = n$ (which correspond to tone frequencies f_n) were determined.

As the airflow speed varies with height in the boundary layer, the phase change of the sound propagating back upstream will vary throughout the boundary layer whereas in the model the sound wave is assumed to propagate back upstream outside the boundary layer. For the cases investigated in this paper because only low Mach number airflows ($U_{\infty,L} \ll c_0$) are of interest here, the variation of the phase of the sound wave vertically

through the boundary layer on the surface of the aerofoil should be relatively small and thus this approximation should be acceptable.

It is assumed that viscosity damps the feedback mechanism so that the T–S wave reinforcement and subsequent growth remains linear. The level of tone produced appears to not be related to the total amplification of the T–S waves which is indicative of a feedback mechanism, for which the level of the tone would be limited by when the feedback loop becomes 'saturated'.

For the method presented here only modes which are amplified up to the trailing edge (from the point of first instability) are considered. Also for all calculations it was assumed that the kinematic viscosity ν was equal to $1.51\times10^{-5}\,\mathrm{m^2\,s^{-1}}$ and that the speed of sound c_0 was equal to $343\,\mathrm{m\,s^{-1}}$.

3. Validation of the model

3.1. Description of validation cases

In this section the models described in Section 2 are used to predict the laminar boundary layer instability tone frequencies for four validation cases. The validation cases are taken from three published investigations and an experimental investigation undertaken by the authors. The empirical models of Brooks et al. [10], Arbey and Bataille [7] and Paterson et al. [1] are also used to predict tone frequencies. The results of all four models are compared to determine how applicable they are to predicting the laminar boundary layer instability noise produced by an arbitrary aerofoil under arbitrary flow conditions (angle of incidence, Reynolds number, etc.).

The four validation cases are summarized in Table 2.

As stated previously, it is assumed that laminar boundary layer instability tones are produced by the feedback mechanism proposed by Arbey and Bataille [7]. The sound pressure spectrum produced by this mechanism consists of a series of approximately evenly spaced tones superimposed on a broadband hump centered on the peak frequency f_s. In each of the studies used for comparison, f_s is defined slightly differently. The various definitions are given below

- In the model presented here it is assumed that f_s is equal to the frequency of maximum T–S wave amplification, which is equal to the frequency of the peak in the broadband hump in the sound pressure spectrum.
- In the model of Brooks et al. [10], f_s refers to the frequency of the peak in the sound pressure level spectrum.
- In Paterson et al.'s [1] equation (Eq. (1)) f_s does not refer to the peak broadband frequency, but rather the frequency of the dominant tone. As noted by Arbey and Bataille [7] the dominant frequency observed by Paterson et al. [1] should indeed be identified with f_s defined here since the broadband contribution, on which the discrete spectrum is superimposed, determines the value of the dominant frequency of the overall noise spectrum.
- Although McAlpine et al. [8] propose a slightly different mechanism by which laminar boundary layer instability noise is produced, they do calculate the frequency of maximum T–S wave amplification (which they assume is the frequency of the tone) for case 2 which is referred to here as f_s.

Table 2
Validation case summary.

	Case 1	Case 2	Case 3	Case 4
Aerofoil	NACA0012	NACA0012	NACA0012	NACA0018
Chord (m)	0.08	0.3	0.229	0.1
U_∞ ($\mathrm{m\,s^{-1}}$)	20.2	29.7	30-60	30
Angle of incidence relative to flow direction	0°	4°	6°	8°
Wind tunnel type	Free-jet	Closed wind tunnel	Free-jet	Free-jet
Results presented in	Ref. [7]	Ref. [8]	Ref. [1]	Present work

3.1.1. Case 1

Arbey and Bataille [7] measured the noise produced by an 80 mm chord aerofoil inclined at 0° to a 20.2 m s^{-1} airflow. As the aerofoil was immersed in a free jet at 0° angle of incidence, no wind tunnel corrections were applied for the calculations presented here. The height of the free jet at the tunnel exit was 150 mm and the aerofoil was mounted in the centre of the free jet.

The sound pressure spectrum contained a series of evenly spaced tones at frequencies f_n, superimposed upon a broadband contribution centered about f_s, and was typical of the laminar boundary layer instability noise spectra produced by the aerofoils Arbey and Bataille [7] investigated. Although they do not record the frequencies of these tones they do give empirical expressions based on the results of a larger experimental investigation which will be used for comparison with the various models.

3.1.2. Case 2

McAlpine et al. [8] and Nash et al. [9] measured the noise produced by a 300 mm chord NACA0012 aerofoil inclined at 4° to the airflow. A single high amplitude tone was observed at 1048 Hz. The boundary layer velocity profiles were measured over the pressure surface of the aerofoil using laser Doppler anemometry and the total T–S wave amplification was calculated using a method similar to that described in Section 2 (a different method of solving the Orr–Sommerfeld equation was used). McAlpine et al. [8] observed a small region of separated flow close to the trailing edge of the aerofoil in which T–S waves underwent large amplification.

The working section of the closed wind tunnel in which the experiments were undertaken had a rectangular cross-section of 0.85 m (wide) × 0.6 m (high) and was 1.5 m long with corner fillets tapering from 0.141 m × 0.106 m at the entry to 0.123 m × 0.093 m at the exit. The wind tunnel corrections applied in the calculations presented here neglect the effect of the corner fillets, i.e., a rectangular tunnel cross section was assumed. The aerofoil was mounted in the centre (height-wise) of the working section and spanned the width of the working section. The wind tunnel velocity was reported by Nash et al. [9] to be 29.7 m s^{-1}.

3.1.3. Case 3

Paterson et al. [1] measured the noise produced by a 9 in. chord NACA0012 aerofoil inclined at 6° to a 30–60 m s^{-1} airflow. They observed that when the frequency of the tones which were produced were plotted against airflow speed the tones arranged themselves into a 'ladder' (see Fig. 1), which for large variations in airflow speed the tone frequency was proportional to $\sim U_\infty^{1.5}$ but for small variations in airflow speed the tone frequency was proportional to $\sim U_\infty^{0.85}$ (these are the 'rungs' of the ladder).

The experiments were undertaken in a free jet of rectangular cross-section 31″ high × 21″ wide × 30″ long. The aerofoil was mounted in the centre (height-wise) and spanned the width of the working section.

3.1.4. Case 4

For this case the noise produced by a 100 mm chord NACA0018 aerofoil inclined at 8° to a 10–40 m s^{-1} airflow is considered. Calculations are presented for only the 30 m s^{-1} case.

The experiments were undertaken, as part of a larger investigation by the authors, within the low-noise wind tunnel in the Department of Mechanical Engineering at the University of Canterbury. The wind tunnel is an open circuit type with testing being undertaken within the exit jet. The maximum airflow speed within the exit jet is 44 m s^{-1} with a turbulence intensity of ~1 percent over the entire airflow speed range. For the experimental work described here the tunnel was significantly modified to reduce the noise level. These modifications included relocating the fans further away from the outlet jet, lining a significant portion of the wind tunnel with sound absorbing material, adding a low frequency absorber section and placing an 'anechoic shelter' over the exit jet to reduce background noise from the rest of the laboratory wing where the wind tunnel is housed. The modifications are described in detail in Kingan and Pearse [33].

The wind tunnel airflow speed for each test was measured using a pitot tube and water micromanometer. The aerofoil was placed in the centre of the free jet, which was square with dimensions 700 mm × 700 mm, and the aerofoil spanned the width of the free jet. No endplates were attached to the aerofoil. The sound pressure level was measured using a Brüel & Kjær 1/2″ microphone (type 4189) placed just outside the airflow directly below the middle of the trailing edge of the aerofoil. The signal from the microphone was fed to a Brüel &

Kjær 2260 sound analyser running BZ 7208 FFT software. The FFT analysis had a frequency resolution of approximately 15 Hz for all tests.

The sound pressure spectrum produced at an airflow speed of $30\,\mathrm{m\,s^{-1}}$ is shown in Fig. 4 (left). A broadband 'hump', and several tones are evident. This is similar to the spectra observed by Arbey and Bataille [7] and was typical of the spectra observed for the experiments described here.

Fig. 4 (right) shows the frequency of the tones produced by the aerofoil versus airflow speed. For cases where more than one tone was observed at a single airflow speed, the frequency of the loudest tone is indicated by a square and the frequency of the other tones is indicated by crosses.

The frequency of the loudest tone varied with $U_\infty^{1.5}$ which is identical to the relationship observed by Paterson et al. [1] and indicated that the tones were being produced by the laminar boundary layer instability noise mechanism.

3.2. Results: case 1

The peak frequency f_s predicted by each of the models is summarized in Table 3. It is assumed that the empirical model of Arbey and Bataille [7] (Eq. (2)) gives an accurate estimate of f_s for this case.

The values of f_s predicted by the models of Paterson et al. [1] and Brooks et al. [10] are in reasonable agreement with the prediction of Eq. (2). However, the value of f_s calculated using the method described in Section 2 was 26 percent higher than that predicted by Eq. (2). The reason for this large difference is possibly due to the inaccurate calculation of the boundary layer growth over the surface of the aerofoil by XFOIL because of the very low Reynolds number. This result represents the largest error in the calculated value of f_s using the method described in Section 2 which the authors have encountered.

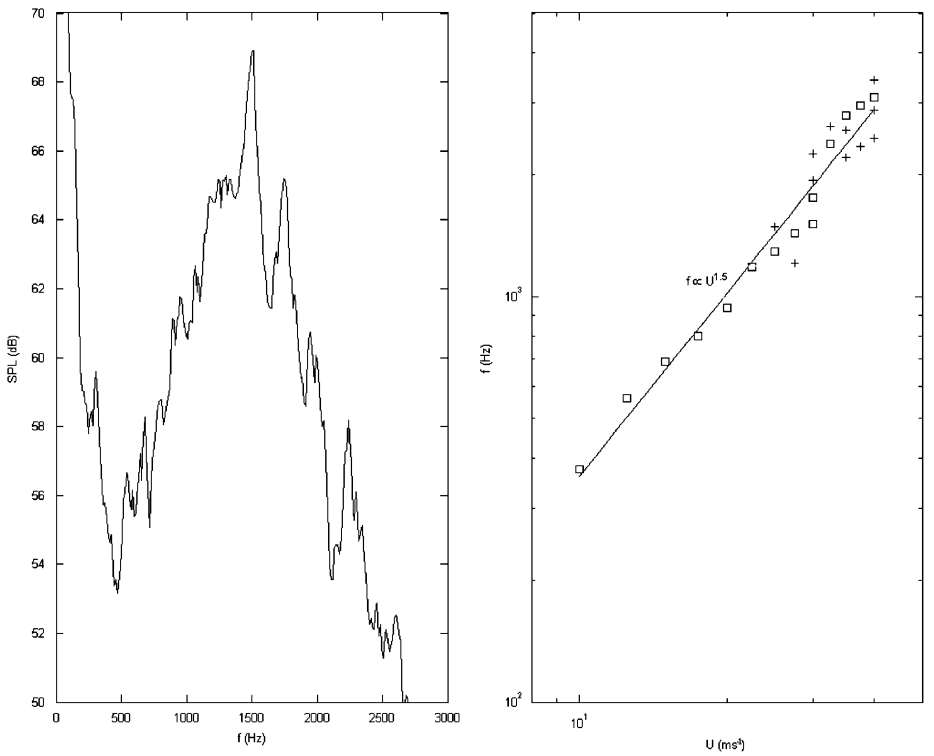

Fig. 4. Sound pressure level versus frequency at $30\,\mathrm{m\,s^{-1}}$ (left); tone frequency versus airflow speed for a 100 mm chord NACA0018 aerofoil inclined at 8° to the airflow (right).

Table 3
Case 1: peak frequency prediction.

Investigator	f_s (Hz)	$f_s/f_{s,\text{Arbey and Bataille}}$
Arbey and Bataille [7]; Eq. (2)[a]	1077	1
Paterson et al. [1]; Eq. (1)	909	0.84
Brooks et al. [10]; Appendix A	1102	1.02
Method described in Section 2	1356	1.26

[a]Assuming $\delta^* = 0.9$ mm from Table 1 in Ref. [7].

Table 4
Case 1: tone frequency prediction.

n see Eq. (33)	7	8	9	10	11	12
f_n (Hz)	1006	1158	1311	1468	1626	1788
$\Delta f = f_{n+1} - f_n$ (Hz)	152	154	156	159	161	

Eq. (4) gives $\Delta f = 166$ Hz (using $L_A = 0.069$ from Table 2 in Ref. [7]) which is in good agreement with the frequency spacing between the tones predicted using the method described in Section 2, which are given in Table 4.

For this case the XFOIL flow simulation predicted a region of mildly separated flow on both surfaces of the aerofoil close to the trailing edge. The calculation of the total amplification over the surface of the aerofoil showed that T–S waves were highly amplified in this separated flow region. This is consistent with the hypothesis of McAlpine et al. [8] and Nash et al. [9] who considered the existence of such a region of separated flow essential for the production of tonal noise. The total T–S wave amplification (A) and the variation of the phase function (F), calculated using the method described in Section 2 are shown in Fig. 5.

3.3. Results: case 2

For this particular case the XFOIL calculation predicted a region of mildly separated flow close to the trailing edge (downstream of 86 percent chord length from the leading edge). Several of the dimensionless Falkner–Skan boundary layer velocity profiles close to the trailing edge, which were fitted to the shape factors predicted by the XFOIL calculation, are shown in Fig. 6.

It is assumed that the peak frequency f_s corresponds closely to the tone frequency $f_{\text{tone}} = 1048$ Hz. The results of the various models for predicting f_s are given in Table 5.

The method described in Section 2 predicted a value for f_s which was in good agreement with that calculated by McAlpine et al. [8] who used experimentally measured boundary layer velocity profiles in their calculation, while the other models gave less accurate predictions of f_s.

McAlpine et al. [8] only observed one tone at 1048 Hz for this case. However, using the method described in Section 2 frequencies at which feedback would occur were calculated. The results are listed in Table 6.

The feedback frequency $f_n = 1042$ Hz corresponded most closely with the tone (at 1048 Hz) observed by McAlpine et al. [8].

As was observed by McAlpine et al. [8] and Nash et al. [9] there were relatively high levels of T–S wave amplification in the regions of mildly separated flow close to the aerofoil trailing edge, which is clearly shown in the plot of T–S wave amplification rates below (Fig. 7).

The XFOIL simulation predicted transition would occur at 98.3 percent chord, which is downstream of the last station used in the calculations presented here (at 98 percent chord). McAlpine et al. [8] also observed that no tone was observed when the aerofoil was inclined at an angle of 3° to the airflow for which XFOIL predicts transition at 96 percent chord length from the leading edge. XFOIL predicts transition using a simple "e^n transition criterion" [20]. Free transition is notoriously difficult to predict and actually occurs over a finite distance, however, for cases where transition is predicted to occur well upstream of the trailing edge (as in the

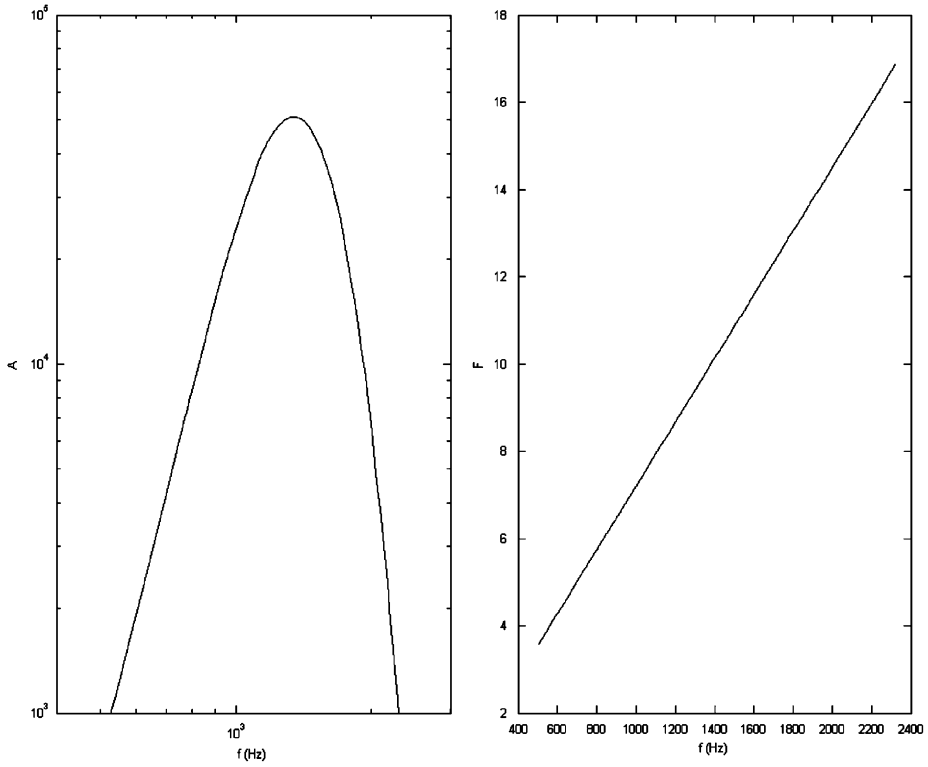

Fig. 5. Total amplification A (left) and phase function F (right).

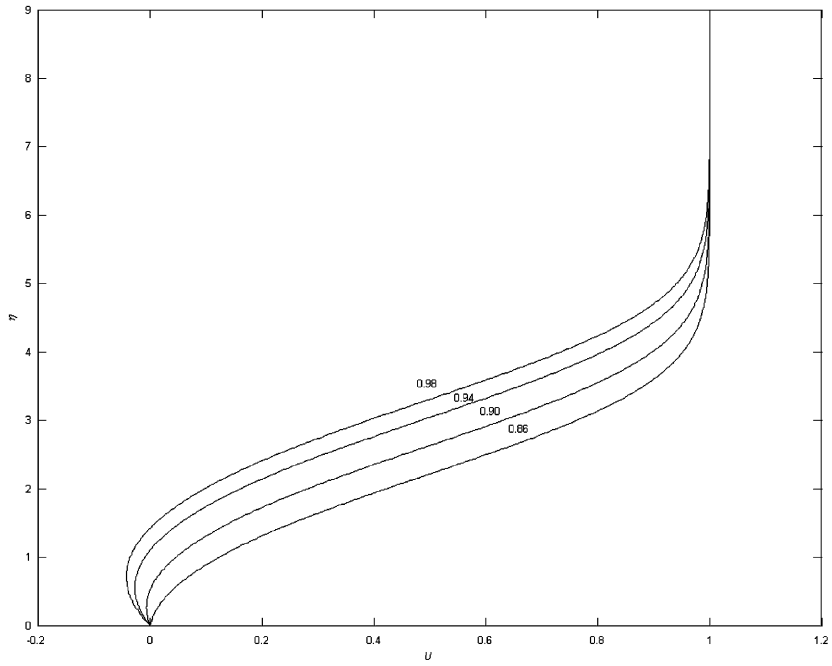

Fig. 6. Dimensionless Falkner–Skan boundary layer velocity profiles at a number of stations close to the trailing edge of the aerofoil (the number adjacent to each curve corresponds to the station position as a fraction of the chord from the leading edge).

Table 5
Case 2: peak frequency prediction.

	f_s (Hz)	f_s/f_{tone}
McAlpine et al. [8] (calculation)	1050	1.00
Arbey and Bataille [7] (Eq. (2)[a]	1521	1.45
Paterson et al. [1] Eq. (1)	853	0.81
Brooks et al. [10] Appendix A	1039	0.99
This paper Eq. (32)	1000	0.95

[a]Using $\delta^*_{\text{TE}} = 0.95\,\text{mm}$ from Eq. (A.5).

Table 6
Case 2: tone frequency prediction.

n (see Eq. (33))	17	18	19	20	21	22
f_n (Hz)	985	1042	1100	1159	1219	1280

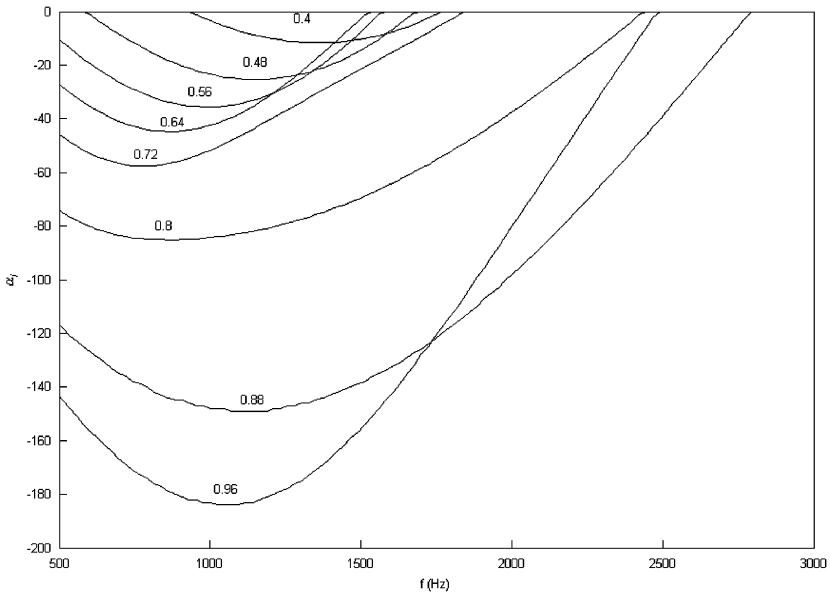

Fig. 7. Local T–S wave amplification rates (α_i) at various chordwise positions along the aerofoil surface (the number adjacent to each curve corresponds to the station position as a fraction of the chord from the leading edge).

3° angle of incidence case) it may be assumed that laminar boundary layer instability noise will not be produced. For cases where transition occurs close to the trailing edge, or where the flow is close to undergoing transition, there will be some uncertainty as to whether laminar boundary layer instability noise will actually occur. Whether it does or not will depend heavily on factors such as the free-stream turbulence level, the roughness of the aerofoil surface and air temperature.

3.4. Results: case 3

The peak frequency f_s predicted using the models of Brooks et al. [10] and the method described in Section 2 are in reasonable agreement with the empirical relationship given by Paterson et al. [1] (Eq. (1)) which was based on the results of this and other experiments. The model of Arbey and Bataille [7] (Eq. (2)) in which δ^*_{TE} was calculated using Eq. (A.5) predicts f_s values which appear to be significantly in error (Fig. 8).

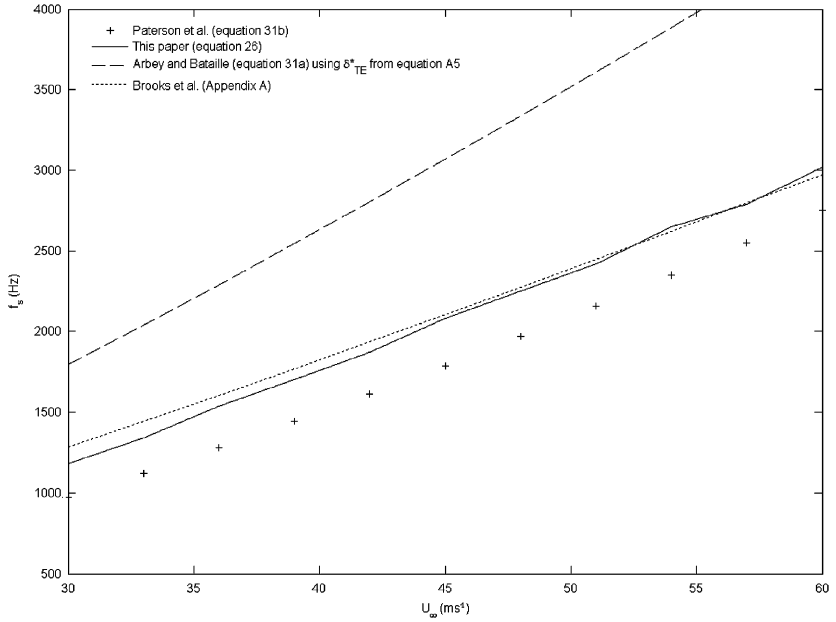

Fig. 8. f_s calculated using a number of different methods.

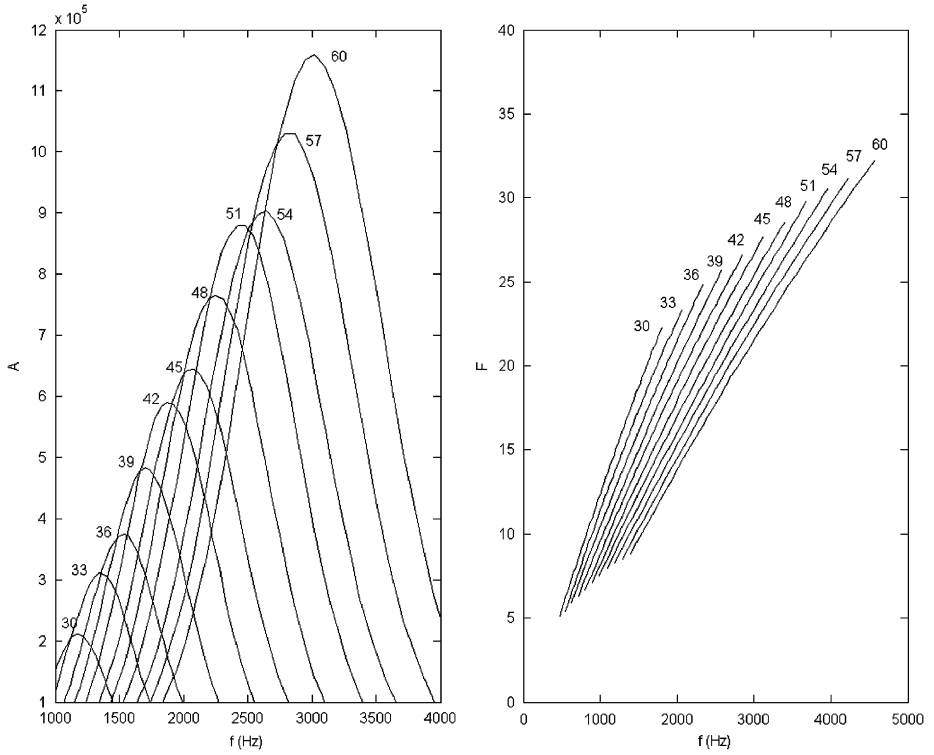

Fig. 9. Total T–S amplification A (left) and phase function F (right) at various airflow speeds (U_∞ in $\mathrm{m\,s^{-1}}$ is indicated by the number adjacent to the curve).

Table 7
Case 3: tone frequency prediction.

U_∞ (m s^{-1})	30	33	36	39	42	45	48	51	54	57	60
Δf (Hz); this paper	78	85	91	97	103	109	116	119	125	129	136
Δf (Hz); Eq. (4)[a]	103	111	120	128	137	145	153	161	169	177	185

[a]Using $L_A = 0.156$ m from [7] Table 2.

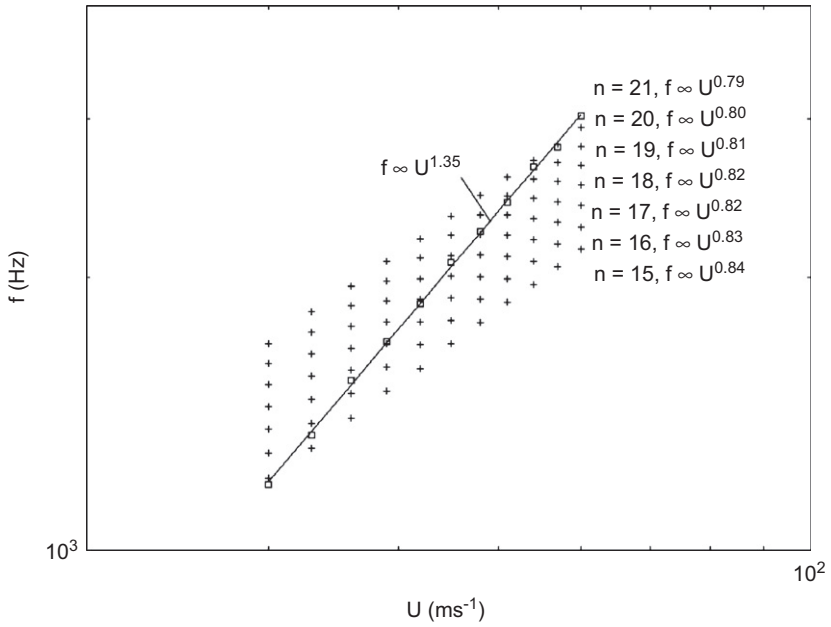

Fig. 10. 'Ladder diagram' calculated using the method described in this paper.

The total T–S wave amplification (A) and the phase function (F), calculated using the methods described in Section 2 for airflow speeds between 30 and 60 m s^{-1} are shown in Fig. 9.

The difference between the two tone frequencies either side of the frequency of maximum T–S wave amplification was taken to be equal to Δf. This is compared with Δf calculated from Eq. (4) in Table 7 and shows moderately good agreement between the two models.

The tone frequencies f_n and frequency of maximum T–S wave amplification f_s predicted by the models developed in this paper are plotted against U_∞ in Fig. 10. The classic 'ladder' diagram is reproduced with the frequency of maximum T–S wave amplification scaling in proportion to $U^{1.35}$, which is close to the $U^{1.5}$ scaling observed by Paterson et al. [1], while the tone frequencies scale in proportion to $U^{0.79–0.84}$, which is close to the $\sim U^{0.85}$ scaling observed by Paterson et al. [1].

As in the previous cases, the XFOIL simulation predicted a region of mildly separated flow close to the trailing edge of the aerofoil on the pressure surface for all airflow speeds. For all cases the T–S waves underwent a relatively high level of amplification in the regions of mildly separated flow.

3.5. Results: case 4

The calculated frequency of maximum amplification was 1760 Hz which is 16 percent higher than the loudest tone observed at 1512 Hz. The four calculated tone frequencies which corresponded most closely with the experimentally observed tones are recorded in Table 8.

Table 8
Case 4: calculated and observed tone frequencies.

n (see Eq. (33))	8	9	10	11
f_n (Hz) calculated	1654	1865	2082	2307
f_n (Hz) experiment	1512	1758	1958	2238

Table 9
Case 4. Peak frequency prediction.

	f_s (Hz)	f_s/f^*_{tone}
Paterson et al. [1]; Eq. (1)	1470	0.97
Brooks et al. [10]; Appendix A	1713	1.13
Method described in Section 2	1760	1.16

f^*_{tone} is the frequency of the loudest tone—1512 Hz.

The frequencies of the tones predicted by the feedback model agree reasonably well with the experimental results. As expected these four tone frequencies corresponded to the highest levels of calculated T–S amplification and corresponded to amplification distances of 8–11 T–S wavelengths.

The peak frequency f_s calculated by the various models are given in Table 9.

The model of Brooks et al. [10] is empirical and was derived from testing exclusively on a NACA0012 aerofoil. Therefore the frequencies predicted by it are only really applicable to tests undertaken on the NACA0012 aerofoil. It is, therefore, somewhat surprising that the model predicts a value for f_s which is reasonably close to the frequency of the loudest tone produced in this experiment. This agreement is most probably just coincidence as the boundary layer thickness at the trailing edge of the NACA0012 aerofoil will be somewhat different to that of the NACA0018 aerofoil. The applicability of Brooks et al.' [10] model to other aerofoil shapes is of interest, as it could be used to predict the frequency of tones produced by aerofoil profiles other than the NACA0012 aerofoil. This is one of the advantages of the model described in this paper, in that as it is purely theoretical, it is applicable to any aerofoil shape and airflow condition. The model of Paterson et al. [1] also predicts a peak which is very close (3 percent lower) to the frequency of the loudest tone which occurred in the experiment.

Again the XFOIL simulation predicted a region of mildly separated flow existed close to the trailing edge on the pressure surface of the aerofoil in which T–S waves underwent a high level of amplification.

4. Recommendations

In experiments undertaken by the authors it was observed that a stalled aerofoil also produced tones which had the same spectral characteristics as the laminar boundary layer instability noise cases considered in this paper. It is therefore reasonable to assume that the tones produced by the stalled aerofoils were due to the laminar boundary layer instability noise mechanism described here. For such cases the authors have had some success in predicting the frequency of the tones using the method described in Section 2 but using commercial CFD software to predict the steady pressure distribution over the aerofoil surface and a boundary layer integral technique to predict the boundary layer profiles over the pressure surface of the aerofoil. However, this method assumes that the pressure distribution on the pressure surface of the aerofoil does not vary significantly with time which may be questionable for a stalled aerofoil.

To speed up the method for practical implementation into an aerofoil noise prediction code, a library of dimensionless T–S wavenumbers α could be determined for a range of different Falkner–Skan boundary layer profiles (similar to those provided in Ref. [34]).

An analysis of the accuracy of the XFOIL transition criterion to determine when laminar boundary layer instability noise will occur is required. Assuming laminar boundary layer instability noise occurs at all Reynolds numbers lower than when transition was predicted to occur at >98 percent chord from the leading edge appeared to work well for the limited number of cases considered here.

5. Conclusions

A theoretical model for laminar boundary layer instability noise proposed by McAlpine et al. [8] and Nash et al. [9] was extended to incorporate a tone selection mechanism based on the feedback mechanism proposed by Arbey and Bataille [7] and was used to predict the frequencies of the tones for a number of cases. The model employed a global method of solving the Orr–Sommerfeld equation which led to easy automation. The models could be used as a predictive tool for laminar boundary layer instability noise on arbitrary aerofoil shapes. This is significant as no accurate method of doing this currently exists for making laminar boundary layer instability noise predictions, (although empirical models exist for the NACA0012 aerofoil).

Supporting the hypothesis of McApline et al. [8] and Nash et al. [9] the XFOIL simulations predicted a region of mildly separated flow close to the trailing edge for all cases investigated in this paper (where laminar boundary layer instability noise was produced). The T–S waves underwent high levels of amplification in these regions of mildly separated flow.

Empirical models were used to predict the laminar boundary layer instability noise produced by a NACA0018 aerofoil. The results are compared with the current model and with an experimental investigation conducted by the authors. The proposed model reasonably accurately predicted the frequency of the tones produced by the aerofoil while the empirical models gave mixed results. The ability of empirical models derived from tests on one aerofoil shape to predict the frequency of laminar boundary layer instability noise was questioned.

Due to the nonlinear nature of the feedback mechanism the level of tones is not related to the level of amplification over the pressure surface of the aerofoil. Thus the model can only be used for predicting frequencies at which tones will occur and could not be extended to predict the level of the tones.

Acknowledgements

The authors acknowledge the support of Hubco Automotive Ltd. and the Foundation for Research, Science and Technology and the Royal Aeronautical Society of New Zealand (by way of the Mercer memorial scholarship).

Appendix A. Model of Brooks et al.

Brooks et al. [10] give the following model for prediction the peak frequency produced by a NACA0012 aerofoil exhibiting laminar boundary layer instability noise. The aerofoil is of chord C, is inclined at angle of incidence α_t, is immersed in a free-jet of height h, speed U_∞ and viscosity ν.

For an aerofoil in a closed wind tunnel α_* is replaced by the angle of incidence of the free equivalent aerofoil (see Section 2.4):

$$f_s = \frac{St' U_\infty}{\delta_P} \tag{A.1}$$

$$St' = St'_1 10^{-0.04\alpha_*} \tag{A.2}$$

$$St'_1 = \begin{cases} 0.18 & R_C \leqslant 1.3\times 10^5 \\ 0.001756 R_C^{0.3931} & 1.3\times 10^5 < R_C \leqslant 4\times 10^5 \\ 0.28 & 4.0\times 10^5 < R_C \end{cases} \tag{A.3}$$

$$\frac{\delta_0}{C} = 10^{1.6569-0.9045\log_{10} R_C+0.0596(\log_{10} R_C)^2}, \quad \frac{\delta_P}{\delta_0} = 10^{-0.04175\alpha_*+0.00106\alpha_*^2} \tag{A.4}$$

$$\frac{\delta_0^*}{C} = 10^{3.0187-1.5397\log_{10} R_C+0.1059(\log_{10} R_C)^2}, \quad \frac{\delta_{\mathrm{TE}}^*}{\delta_0^*} = 10^{-0.0432\alpha_*+0.00113\alpha_*^2} \tag{A.5}$$

$$R_C = U_\infty C/\nu, \quad \alpha_* = \frac{\alpha_t}{\eta}, \quad \eta = [(1+2\sigma)^2 + \sqrt{12\sigma}], \quad \sigma = \left(\frac{\pi^2}{48}\right)\left(\frac{C}{h}\right)^2 \tag{A.6}$$

References

[1] R.W. Paterson, P. Vogt, M. Fink, C. Munch, Vortex noise of isolated airfoils, *AIAA paper 72–656, also appearing in revised form in the Journal of Aircraft* 10 (1973) 296–302.

[2] C.K.W. Tam, Discrete tones of isolated airfoils, *Journal of the Acoustical Society of America* 55 (1974) 1173–1177.

[3] H. Schlichting, *Boundary Layer Theory*, sixth ed., Springer, Berlin, 1968.

[4] S.E. Wright, The acoustic spectrum of axial flow machines, *Journal of Sound and Vibration* 45 (1976) 165–223.

[5] R.E. Longhouse, Vortex shedding noise of low tip speed axial flow machines, *Journal of Sound and Vibration* 53 (1977) 25–46.

[6] M.R. Fink, Fine structure of airfoil tone frequency, Paper H3, presented at the 95th meeting of the Acoustical Society of America, 1978.

[7] H. Arbey, J. Bataille, Noise generated by airfoil profiles placed in a uniform laminar flow, *Journal of Fluid Mechanics* 134 (1983) 33–47.

[8] A. McAlpine, E.C. Nash, M.V. Lowson, On the generation of discrete frequency tones by the flow around an aerofoil, *Journal of Sound and Vibration* 222 (1999) 753–779.

[9] E.C. Nash, M.V. Lowson, A. McAlpine, Boundary layer instability noise on aerofoils, *Journal of Fluid Mechanics* 382 (1999) 27–61.

[10] T.F. Brooks, D.S. Pope, M.A. Marcolini, Airfoil self-noise and prediction, NASA RP-1218, 1989, pp. 1–137.

[11] C. Mari, D. Jeandel, J. Mathieu, Méthode de calcul de couche limite turbulente compressible avec transfert de chaleur, *International Journal of Heat and Mass Transfer* 19 (1976) 893–899.

[12] C. Henry, Solution numéric par une méthode de singularités du bruit de profil l'écoulement compressible sur des surfaces de courant axi-symétriques, Thése de Docteur Ingénieur, Université Claude Bernard, Lyon I, 1975.

[13] H. Arbey, Contribution á l'étude des mécanismes de l'émission sonore de profiles aérodynamiques places dans des écoulements sains ou perturbés, Thése de Doctorat és Sciences, Université Claude Bernard, Lyon I, 1981.

[14] I. Dolgova, Sound field radiated by a T–S wave, *Soviet Physics—Acoustics* 23 (1977) 259.

[15] T.R. Akylas, N. Toplosky, The sound field of a T–S wave, *Physics of Fluids* 29 (1986) 685.

[16] J. Laufer, T.-C. Yen, Noise generated by a low Mach number jet, *Journal of Fluid Mechanics* 134 (1983) 1–31.

[17] D.G. Crighton, P. Huerre, Model problems for the generation of superdirective acoustic fields by wave packets in shear layers, AIAA-84-2295, 1984.

[18] L.B. Aizin, Sound generation by a Tollmien–Schilichting wave at the end of a plate in a flow, *Tekhnicheskaya Fizika* 3 (1992) 50–57 (Translated from Prikladnaya Mekhanika).

[19] F.S. Archibald, The laminar boundary layer instability excitation of an acoustic resonance, *Journal of Sound and Vibration* 38 (1975) 387–402.

[20] M. Drela, XFOIL: an analysis and design system for low Reynolds number airfoils, *Conference on Low Reynolds Number Airfoil Aerodynamics*, University of Notre Dame, June 1989.

[21] M. Drela, M.B. Giles, Viscous-inviscid analysis of transonic and low Reynolds number aerofoils, *AIAA Journal* 25 (1987) 1347–1355.

[22] T. Cebeci, H.B. Keller, Shooting and parallel shooting methods for solving the Falkner–Skan boundary layer equations, *Journal of Computational Physics* 7 (1971) 289–300.

[23] H. Haj-Hariri, Transformations reducing the order of the parameter in differential eigenvalue problems, *Journal of Computational Physics* 77 (1988) 472–484.

[24] L. Trefethan, *Spectral Methods in Matlab*, SIAM, Philadelphia, 1998.

[25] V. Theofilis, Spectral collocation and the Orr–Sommerfeld stability equation, *Journal of Engineering Mathematics* 28 (1994) 241–259.

[26] B.S. Ng, W.H. Reid, An initial value method for eigenvalue problems using compound matrices, *Journal of Computational Physics* 30 (1979) 125–136.

[27] T.J. Bridges, P.J. Morris, Differential eigenvalue problems in which the parameter appears nonlinearly, *Journal of Computational Physics* 55 (1984) 437–460.

[28] D.S. Henningson, P.J. Schmidt, *Stability and Transition in Shear Flows*, Springer, New York, 2001.

[29] R. Jordinson, The flat plate boundary layer. Part 1: numerical integration of the Orr–Sommerfeld equation, *Journal of Fluid Mechanics* 43 (1970) 801–811.

[30] T.F. Brooks, M.A. Marcolini, Airfoil trailing edge flow measurements and comparison with theory incorporating open wind tunnel corrections, *Presented at the 9th AIAA/NASA Aeroacoustics Conference*, Williamsburg, Virginia, 1984.

[31] H.J. Allen, W.G. Vincenti, Wall interference in two-dimensional-flow wind tunnel with consideration of effect of compressibility, NACA report 782, 1944.
[32] J.C. Yu, C.K.W. Tam, Experimental investigation of the trailing edge noise mechanism, *Journal of the AIAA* 16 (1977) 1046–1052.
[33] M.J. Kingan, J.R. Pearse, Development of a low-noise wind tunnel, *Presented at Internoise 2005*, Rio de Janeiro, Brasil, paper No. 2090, 7–10 August 2005.
[34] H.J. Obremski, M.V. Morkovin, M. Landahl, A.R. Wazzan, T.T. Okamura, A.M.O. Smith, A portfolio of stability characteristics of incompressible boundary layers, AGARDograph 134, 1969.